Published in IET Microwaves, Antennas & Propagation
Received on 5th November 2009
Revised on 14th May 2010
doi: 10.1049/iet-map.2009.0543

In Special Issue on Microwave Metamaterials: Application to Devices, Circuits and Antennas

ISSN 1751-8725

Wide angle impedance matching metamaterials for waveguide-fed phased-array antennas

S. Sajuyigbe[1] *M. Ross*[1] *P. Geren*[2] *S.A. Cummer*[1]
M.H. Tanielian[2] *D.R. Smith*[1]

[1]*Department of Electrical and Computer Engineering, Center for Metamaterials and Integrated Plasmonics, Duke University, Durham, NC 27708, USA*
[2]*Boeing Phantom Works, P.O. Box 3999, MC 3W-81 Seattle, WA 98124-2499, USA*
E-mail: ajs35@duke.edu

Abstract: This work investigates the gains realisable through the use of artificially structured materials, otherwise known as metamaterials, in the wide angle impedance matching (WAIM) of waveguide-fed phased-array antennas. The authors propose that the anisotropic properties of a metamaterial layer, when designed appropriately, can be employed to achieve impedance matching at a wide contiguous range of phased-array antenna transmission angles. Simulation and numerical results show that an optimised impedance match over a broad angular range can be readily achieved using a doubly uniaxial (magnetic and electric) anisotropic layer, an outcome not found accomplishable when an optimised isotropic dielectric layer is used. The authors propose the possibility of using metamaterials to achieve anisotropic WAIM layer configurations, and the authors show, using two simple uniaxial designs, that a metamaterial layer over the phased-array gives performance characteristics similar to its homogeneous anisotropic effective medium counterpart.

1 Introduction

Since the inception of research in the area of metamaterials, researchers have explored the various advantages that these novel, artificially structured materials may provide [1–6]. Beginning with the first experimental works on these materials [7, 8], it has been established that metamaterials can indeed display properties that are difficult or impossible to achieve in conventional materials. Combined with the ease of design, very sophisticated devices, such as the invisibility cloak [9], can be created.

In electromagnetic devices, in which conventional dielectrics are used, the use of carefully designed metamaterials can potentially improve engineering designs thereby leading to enhanced system performance. In this paper, we seek to evaluate the impact of metamaterials as wide angle impedance matching (WAIM) elements in phased-array antennas. To address reflections at the aperture–air interface of waveguide-fed phased-array antennas, a matching WAIM structure (usually made up of a stack of dielectric layers) is one method employed to offset the encountered mismatch [10]. In order to achieve a wide angular range of maximal transmission (or minimal return loss) for the array, an optimisation is performed to vary the dielectric values and thicknesses of one or more WAIM layers until an acceptable return loss is achieved. Depending on the antenna geometry and operating frequency, however, it often becomes difficult to match the antenna at all angles using the limited set of dielectric materials available in nature. To alleviate this problem, one might be able access a wider dielectric range as done in [11], or better yet even utilise (if accomplishable) materials with which one can simultaneously access anisotropic magnetic and dielectric properties whose μ or ϵ in all cartesian directions can be precisely engineered. By providing several controllable variables, the latter would increase the ease of matching waveguide-fed array antennas

to free space at all scan angles. We propose using metamaterials as anisotropic WAIM layers, as these materials can be used to access and engineer anisotropic magnetic and dielectric constitutive parameters.

We thereby extend the previously existing method of dielectric WAIM layer optimisation to allow a wider range of μ and ϵ, and to include anisotropic values of ϵ and μ, a configuration physically accomplishable through the use of metamaterials. The following sections analyse the feasibility of anisotropic metamaterial WAIMs. Section 2 briefly overviews the utility of phased-array antennas and introduces the concept of active element admittance, Section 3 discusses the general impedance matching methodology used later in this document, Section 4 presents results that show the superior performance achievable using anisotropic WAIMs and Section 5 demonstrates the validity of treating metamaterials placed over phased-array antennas as anisotropic WAIM layers.

2 Phased-array antenna overview

A phased-array antenna is a periodic arrangement of antennas that serves the purpose of generating a highly directioinal radiation whose scan direction can be controlled by the phase gradient applied across the array. As shown in Fig. 1, a common phased-array configuration consists of an array of open-ended waveguides in which each waveguide is affixed onto openings in a large perfect electric conductor (PEC) plane with openings having exactly the same dimensions as the open end of the waveguide.

It is desired that the ratio of radiated (transmitted) power to input power be maximised at all output scan angles of the phased-array antenna; this output to input ratio, in the far field of an infinite (or very large) array, is approximately [12, 13]

$$\frac{P_r(\theta, \phi)}{P_i} = (1 - |\Gamma(\theta, \phi)|^2) f(\theta) \tag{1}$$

$f(\theta)$ is a physical limitation that represents the reduction in effective aperture cross section as the beam is steered to angles away from the normal, which varies based on geometric considerations as $\cos\theta$, $(\cos\theta)^{3/2}$, or $(\cos\theta)^2$, depending on the azimuthal plane of scan and the mode distribution of the antenna element [14]. The output transmitted power is dependent on the reflection coefficient $\Gamma(\theta)$ and on the effective aperture cross section, $f(\theta)$. The reduction of the effective aperture size is a physical limitation, therefore it is especially important to minimise $\Gamma(\theta)$ over a very broad range of angles, particularly at large angles. One aforementioned method of minimising the return loss in waveguide-fed phased-array systems is to utilise a combination of isotropic planar dielectric layers placed over the array system [10]. These layers are used to optimise the matching over a band of angles, but the performance achieved using this method, however, is constrained by the inability to implement layers with arbitrarily chosen constitutive parameters.

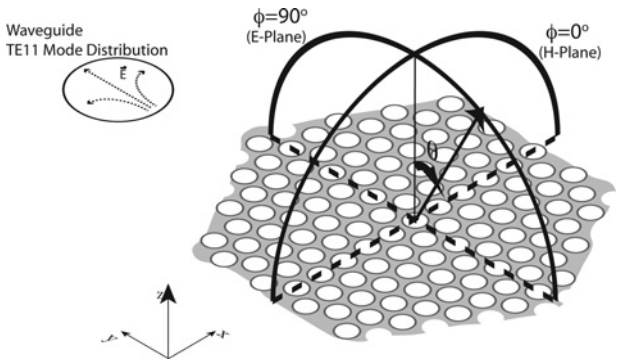

Figure 1 *Array topology*

2.1 Phased-array antenna active element admittance

The active element admittance of an infinite array is the admittance at the aperture–air interface of a single element at the centre of the array when all of the elements in the array are radiating [13]. The active element admittance includes all of the interactions because of other elements in the array. The disparity between the active element admittance (looking out from the aperture discontinuity of the centre element) and the waveguide propagating mode admittance indicates the level of impedance mismatch of the array, which varies as a function of scan angle.

Because the phasing relationship between any two adjacent waveguide elements changes when the scan angle is changed, the mutually induced voltages and subsequently the active element admittance will change when the scan angle is varied. It is therefore necessary to design a stack of WAIM layers that allow reflectionless transmission of the power emanating from the array apertures.

In Section 4, we shall compute the active element admittance for a waveguide-fed antenna array system and prescribe the anisotropic material parameters ($\mu_x = \mu_y$, μ_z, $\epsilon_x = \epsilon_y$, ϵ_z, and thickness, d) of the matching WAIM layer. The obtained results are compared with the impedance matching obtained when using a regular dielectric layer (ϵ, d), instead of an anisotropic layer.

2.2 Calculating the active element admittance

Before exploring the possible advantages presented through the use of metamaterials, we briefly present the method by which the active element admittance has heretofore been calculated, we also present our proposed modifications that take into account the dispersion relation of uniaxial magnetic and dielectric anisotropic WAIM layers.

The active element admittance as a function of scan can be computed using computational tools such as the finite

doi: 10.1049/iet-map.2009.0543

element method solver Ansoft HFSS, or the finite difference time domain solver Microwave Studio CST. Although these programs are precise and can handle arbitrary geometry, full wave simulations are time consuming and not appropriate for the rapid optimisation necessary for wide angle matching. To save computation time, we utilise an analytical approach, discussed hereafter, to obtain the active element admittance as a function of scan.

Various approaches for analytically computing the active element admittance of phased-arrays have been explored in the literature. For large arrays, an infinite element array can be assumed because of its simplicity and accuracy in describing large arrays [13, 15]. All elements are thus assumed to be exactly identical in large arrays since most elements except the edge elements would possess similar admittance and field characteristics when radiating [15, 16].

Several approaches have been proposed for the derivation of the active element admittance of waveguide-fed phased-arrays [12, 15–20]. We utilise the method proposed in [20] to solve for the active element admittance. The method in [20] (just as some of the other cited methods) incorporates both the contribution of higher order waveguide modes in the waveguide and higher order evanescent free space modes just above the aperture discontinuity; Borgiotti [20] has been found to be accurate in predicting phased-array antenna performance, and it is straightforwardly implementable for array with waveguide elements for which the Fourier transform of the eigenmode field distributions are known.

For a given phased-array topology, the approach in [20] represents the fields above the each aperture by a Fourier series summation of plane wave modes with unknown complex amplitudes in the Hilbert space; these are also known as Floquet modes [20, 21]. These fields are boundary matched to the summation of waveguide modes that exist inside each waveguide element, just below the aperture interface. The analytical representation of these fields are shown in the Appendix.

The following set of equations show how Y_{in} may be calculated using the method proposed in [20]

$$V_o Y_{\text{in}}(\boldsymbol{u}_o) - \sum_{i=0}^{N-1} V_i Y_{0i}(\boldsymbol{u}_o) = 0 \tag{2}$$

$$V_k Y_k + \sum_{i=0}^{N-1} V_i Y_{ki}(\boldsymbol{u}_o) = 0 \tag{3}$$

where

$$Y_{ki}(\boldsymbol{u}_o) = \frac{4\pi^2}{C} \sum_{\boldsymbol{u}_{opq}} [\xi^*_{k\rho}(|\boldsymbol{u}_{opq}|)\xi_{i\rho}(|\boldsymbol{u}_{opq}|)Y_{\text{TM}}(|\boldsymbol{u}_{opq}|) - \xi^*_{k\psi}(|\boldsymbol{u}_{opq}|)\xi_{i\psi}(|\boldsymbol{u}_{opq}|)Y_{\text{TE}}(|\boldsymbol{u}_{opq}|)] \tag{4}$$

and

$$\boldsymbol{u}_o = \hat{x}k_x + \hat{y}k_y \tag{5}$$

$$\boldsymbol{u}_{opq} = \boldsymbol{u}_o + p\boldsymbol{t}_1 + q\boldsymbol{t}_2 \tag{6}$$

$$k_x = k_o \sin\theta\cos\phi \tag{7}$$

$$k_y = k_o \sin\theta\sin\phi \tag{8}$$

In the above equations, $\boldsymbol{u}_{opq}$ represents the lattice of free space modes over the array aperture and $Y(\boldsymbol{u}_o)$ represents the active element admittance at some scan angle $\boldsymbol{u}_o$. Vectors $\boldsymbol{t}_1$ and $\boldsymbol{t}_2$ represent the periodicity of the array lattice in the reciprocal space, whereas the p and q scalars are indices that point to contributions from evanescent or propagating plane waves in space, just above the aperture. Y_{ki} is the cross polarisation admittance between different modes in the waveguide element, whereas Y_k in (2) represents the modal admittance (a function of frequency but not scan angle) of waveguide mode k. Indices i and k point to contributing waveguide modes from the fundamental propagating mode at $i = 0$ or $k = 0$ to the least contributive non-propagating mode at $i = \infty$ or $k = \infty$. The summations in (2) and (3) are truncated at a finite $N - 1$ to reflect the negligible contribution of far away higher order modes. Observe that when $i = k = 0$, Y_{00} reduces to the oversimplified case where the influence of only one waveguide mode is being considered, exactly analogous to (12) in [17], this is known as the grating lobe series. The ξ quantity in (4) is the Fourier transform of the field distribution of the kth or ith mode away from cutoff in the waveguide, whereas the ρ and ψ subscripts correspond to the radial and circumferential components of the Fourier transform of the waveguide mode in question.

We utilise the approach shown in (2)–(8) but also make modifications so that the approach accurately characterises the array in the presence of uniaxial ($\mu_x = \mu_y$, μ_z, $\epsilon_x = \epsilon_y$, ϵ_z) anisotropic matching layers. The incorporated modifications are shown in the following set of equations, and are directly derived from the Maxwell's equations

$$Y_{\text{TE}}(|\boldsymbol{u}_{opq}|) = -\frac{H_x}{E_y} = \frac{k_{z,TE}}{\omega\mu_o\mu_x} \tag{9}$$

$$k_{z,\text{TE}} = \sqrt{\omega^2\mu_o\mu_x\epsilon_o\epsilon_y - k_t^2\frac{\mu_x}{\mu_z}} \tag{10}$$

$$Y_{\text{TM}}(|\boldsymbol{u}_{opq}|) = \frac{H_y}{E_x} = \frac{\omega\epsilon_o\epsilon_x}{k_{z,TM}} \tag{11}$$

$$k_{z,\text{TM}} = \sqrt{\omega^2\epsilon_o\epsilon_x\mu_o\mu_y - k_t^2\frac{\epsilon_x}{\epsilon_z}} \tag{12}$$

where

$$k_x = k_o \sin(\theta)\cos\phi$$
$$k_y = k_o \sin(\theta)\sin\phi \quad (13)$$
$$k_t = |\hat{x}k_x + \hat{y}k_y + p\boldsymbol{t}_1 + q\boldsymbol{t}_2|$$

For infinitely thick anisotropic layers placed directly above the aperture–air discontinuity, the admittance parameters Y_{TE} and Y_{TM} above are perfectly valid, for layers of finite thicknesses however, a transmission line impedance transformation equation [22] may be used to recursively transform the Y_{TE} or Y_{TM} from the material at $z = \infty$ to the material at the $z = 0$ plane (see Fig. 1) of aperture discontinuity. This shall be the equivalent effective Y_{TE} and Y_{TM} to be used in (4).

2.3 Verification of quasi-analytical model

A MATLAB program was written to implement the active element admittance for the waveguide-fed phased-array antenna system here analysed. The lattice dimensions of the array are of a typical but arbitrary antenna array configuration and are shown in Figs. 1 and 2 (unit element lattice: waveguide loaded with $\epsilon_r = 2.54$ dielectric opens out of a PEC plane). Each waveguide in the array is cross-fed to excite two orthogonal instances of the fundamental TE_{11} mode (the TE_{11} mode configuration shown in Fig. 1 is the reference mode used for Y_{in} calculations in this paper).

For the analytical model, 49 free space modes are included (i.e. $p = q = [-3, -2, -1, 0, 1, 2, 3]$), and the maximum number of waveguide modes, N, included in the summations of (2) and (3) is ten. It was found that additional Floquet terms over 49 were negligible contributors to Y_{in}; the first ten waveguide modes included are: TE_{11}, TM_{01}, TE_{21},TM_{11}, TE_{01}, TE_{31} and the cross polarised TE_{11} (90° offset), TE_{21} (45° offset), TM_{11} 90° offset) and TE_{31} (30° offset). Other higher order waveguide modes beyond the first ten were found to make negligible contributions.

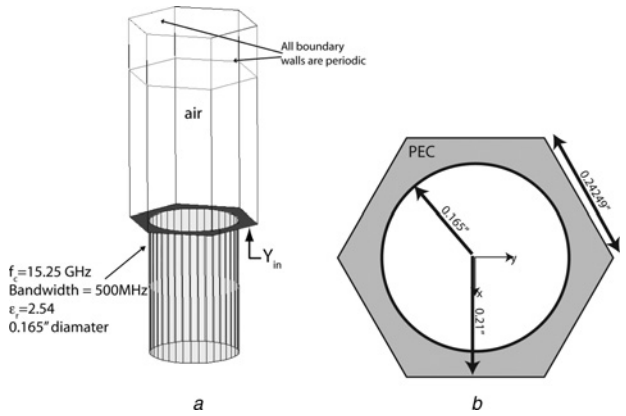

Figure 2 *Pictorial representation of unit lattice*

a Computational domain used in HFSS simulations
b Top view of a single-element lattice

$\xi_{i\psi}$ in (4) represents the Fourier transform of the TE polarised component (with respect to the z-direction) of the ith TE_{np} mode away from the fundamental propagating waveguide mode, whereas ξ_{ip} is the same for the TM polarised component of the same mode. Accordingly, $\xi_{0\psi}$ or $\xi_{0\rho}$ would each represent the TE and TM polarised components of the fundamental TE_{11} mode. Note that the expression for $\xi_{i\psi}$ is printed incorrectly in [20] but is displayed here in its corrected form

$$\xi_{\psi}(t, \mu) = j^{(n-1)} \frac{\sqrt{2/\pi}}{\sqrt{(x'_{np})^2 - n^2}} \frac{a\cos n\mu}{1 - (at/x_{np})^2} J'_n(at) \quad (14)$$

With the inclusion of multiple waveguide modes, the admittance can be expressed as a matrix that contains various higher order free space and waveguide mode terms. For each angle, each of these terms is straightforwardly obtained from (4), and then used in (2) and (3) to generate a matrix that can be solved to compute the input admittance $Y_{\mathrm{in}}(\theta, \phi)$ [expressed as $Y_{\mathrm{in}}(\boldsymbol{u}_o)$ in (2), also see (22) in [20]].

For the geometry assumed in Fig. 2

$$k_t = \left|\hat{x}\left(k_x + p\frac{2\pi}{L}\right) + \hat{y}\left(k_y + \frac{2\pi}{L}\left[p\frac{-1}{\sqrt{3}} + q\frac{2}{\sqrt{3}}\right]\right)\right| \quad (15)$$

In Fig. 3 the accuracy of the MATLAB model with and without higher order modes are compared to the corresponding HFSS results. An infinite phased-array antenna is implemented in HFSS by performing a 3D simulation of single array element unit cell and setting master–slave periodic boundaries on the all the walls of the

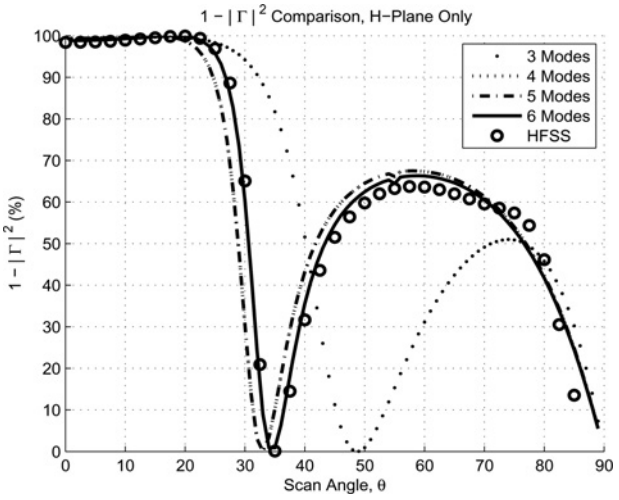

Figure 3 *Effects of the inclusion of higher order waveguide modes on the accuracy of quasi-analytical code*

WAIM layer: $\mu_x = \mu_y = 2$, $\mu_z = 1$, $\epsilon_x = \epsilon_y = 4.2$, $\epsilon_z = 2$, and $d = 2$ mm

doi: 10.1049/iet-map.2009.0543

region above the aperture plane. In HFSS, the $Y_{in}(\phi, \theta)$ (or $\Gamma_{in}(\phi, \theta)$ or $S_{11}(\phi, \theta)$) is obtained by referencing it to the aperture–air discontinuity and not the port assignment at the base of the waveguide.

Fig. 3 shows the results for a phased-array topology with a single layer having $\mu_x = \mu_y = 2$, $\mu_z = 1$, $\epsilon_x = \epsilon_y = 4.2$, $\epsilon_z = 2$, and thickness, $d = 2$ mm placed directly over the aperture face. The comparisons test the accuracy of the MATLAB model of the phased-array antenna active element admittance.

3 Matching of phased-array antenna using anisotropic layers

3.1 WAIM layer optimisation methodology

In order to obtain an ideally matched phased-array antenna structure, the active element admittance at the waveguide junction must equal the admittance of the propagating mode in the waveguide, which, for all scan angles, must be forced to fulfill

$$Y_{in}(\phi, \theta) = Y_{TE_{11}} \tag{16}$$

Because the active element admittance for an anisotropic material layer does not result in a simple analytical expression, an optimisation program was written to choose the constitutive parameters that minimise the reflection coefficient over a broad range of angles, thereby minimising ideally

$$\int_{\phi=0^\circ}^{90^\circ} \int_{\theta=0^\circ}^{90^\circ} \left| \frac{Y_{TE_{11}} - Y_{in}(\phi, \theta)}{Y_{TE_{11}} + Y_{in}(\phi, \theta)} \right|^2 d\theta \, d\phi \tag{17}$$

We implement the `fmincon` constrained optimisation routine in the MATLAB optimisation toolbox to minimise the 'area under the curve' of the integrand in (17). `fmincon` accepts a variety of inputs: it accepts the parameterised function that needs to be optimised, the range of design variables that give flexibility to the problem (which in the uniaxial case are μ_x, μ_z, ϵ_x, ϵ_z and the thickness d of the layer). A constrained optimisation routine is used because we limit the search range for μ, ϵ and thickness d. `fmincon` uses line-search, quasi-newton and sequential programming algorithms to numerically home in on the minimum but needs a given starting point from which it begins its search. Since the optimisation routine does not always arrive at the absolute minimum of the expression in (17), 500 sets of randomly generated starting points (i.e. μ_x, μ_z, ϵ_x, ϵ_z and d) are used to arrive at 500 minima. The smallest local minimum of all the 500 minima is chosen to be the absolute minimum (note that many of the minima in the optimisation search are identical).

A rudimentary pseudocode of the optimisation and implementation code is presented

```
predefine constants: frequency, c, k_o, k_t, ...
predefine variables: waveguide modes,
  Floquet modes, angle range;
get_all_grating_lobe_series();
starting_vars = random('unif', range, 500, ...)

for index = 1:500
[optimised_vars, Integral_value] =
fmincon(@Integral_ReflCoeff_AllAngles, ...);
vars_and_integral = [optimised_vars,
  Integral_value];
sort(vars_and_integral);
end
return vars_and_integral(1, :);
```

4 Results

4.1 Optimising with anisotropic WAIM layer at multiple azimuthal planes

Using the optimisation methodology heretofore discussed, we choose to optimise the phased-array antenna of Figs. 1 and 2 on all azimuthal planes. Since phased-array designers often look at the H-, D- and E-planes [$\phi = 0^\circ$, $\phi = 45^\circ$ and $\phi = 90^\circ$, respectively (see Fig. 1)] to approximately characterise the behaviour of a phased-array system [23], we attempt to simultaneously optimise at all three azimuthal planes and compare results realised when an optimised homogeneous anisotropic layer against when an optimised isotropic dielectric layer is used. The objective function is

$$\sum_{b=0}^{b=2} \sum_{\theta=0^\circ}^{80^\circ} \left| \frac{Y_{TE_{11}} - Y_{in}(45b^\circ, \theta)}{Y_{TE_{11}} + Y_{in}(45b^\circ, \theta)} \right|^2 \tag{18}$$

The constitutive parameters that give an optimised admittance for these planes were once again generated by a MATLAB script incorporating the developments from Sections 2 and 3. Note that the discrete summation in (18) is as effective but not as time-intensive as its continuous integral version in (17). The range allowed for the homogeneous anisotropic parameters was from 0.2 to 5 for ϵ and μ and from 1 to 5 mm for d, whereas the range for the isotropic dielectric was from 1 to 10 for ϵ_r and from 1 to 10 mm for d.

The results of the optimisation for the anisotropic layer and that of the isotropic dielectric layer are shown, respectively, in Figs. 4–6. For the homogeneous anisotropic layer, the optimised WAIM layer parameters are found to be $\mu_x = \mu_y = 1.48$, $\mu_z = 1.97$,

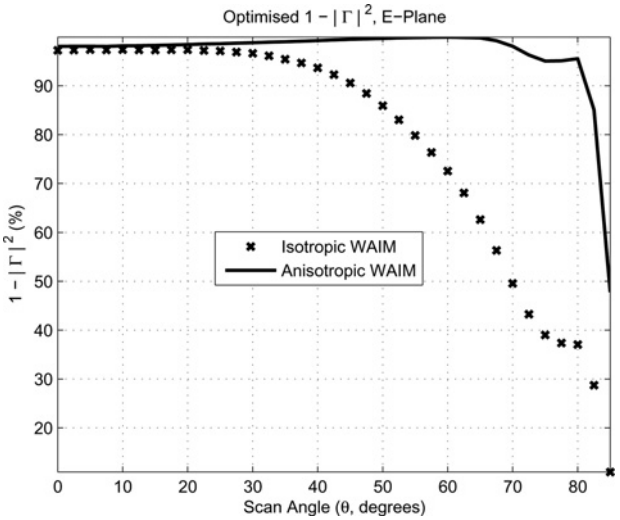

Figure 4 *E-plane ($\phi = 90^\circ$) optimised transmittance for single layer WAIM*

Anisotropic: $\mu_x = \mu_y = 1.48$, $\mu_z = 1.97$, $\epsilon_x = \epsilon_y = 2.34$, $\epsilon_z = 0.74$, $d = 3.1$ mm. Isotropic: $\epsilon_r = 2$ and $d = 2$ mm

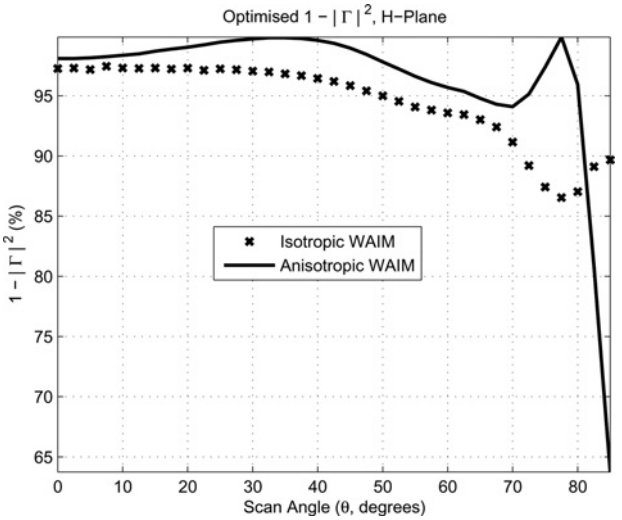

Figure 6 *H-Plane ($\phi = 0^\circ$) optimised transmittance for single layer WAIM*

Anisotropic: $\mu_x = \mu_y = 1.48$, $\mu_z = 1.97$, $\epsilon_x = \epsilon_y = 2.34$, $\epsilon_z = 0.74$, $t = 3.1$ mm. Isotropic: $\epsilon_r = 2$ and $d = 2$ mm

$\epsilon_x = \epsilon_y = 2.34$, $\epsilon_z = 0.74$, $d = 3.1$ mm, while, for comparison, the optimised WAIM parameters using an isotropic dielectric are $\epsilon_r = 2$ and $d = 2$ mm. Using the aniotropic layer, a near-perfect impedance matching is obtained at all the shown azimuthal planes. It is evident from a comparison of Figs. 4–6 that the use of anisotropic layers (which we show to be accomplishable using metamaterials, see Section 5) as opposed to isotropic dielectrics can provide significantly improved transmittance characteristics for a phased-array antenna system. It is important to note that the isotropic dielectrics used for Figs. 4–6 results are best case scenarios that assume that the designer has access to dielectrics with arbitrary ϵ_r, which in actuality is not true. This suggests that the use of anisotropic material layers, if accomplishable, could be promising for the impedance matching of phased-array antennas.

To evaluate the sensitivity of the array transmittance to deviations in anisotropic WAIM values, in Fig. 7 we present results for the performance of the optimised anisotropic WAIM of Figs. 4–6 when $\mu_x (= \mu_y)$ and $\epsilon_x (= \epsilon_y)$ deviate by ten percent from 1.48 and 2.34 to 1.63 and 2.1. The results of Fig. 7 show that the strongly transmissive performance of the anisotropic WAIM is nonetheless retained even when a 10% variation is introduced to some of its constitutive parameters.

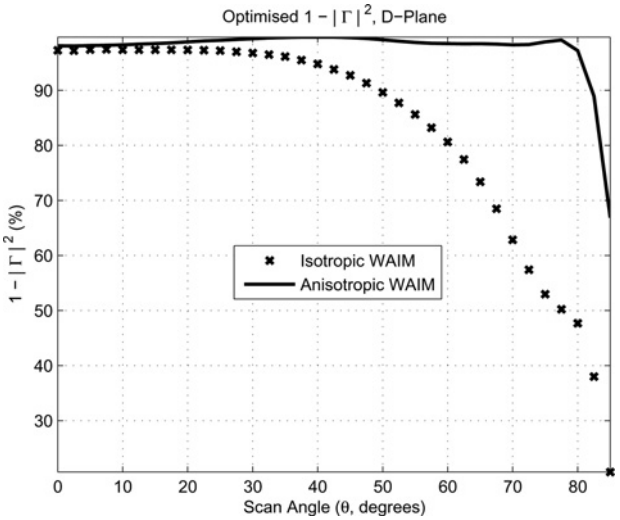

Figure 5 *D-plane ($\phi = 45^\circ$) optimised transmittance for single layer WAIM*

Anisotropic: $\mu_x = \mu_y = 1.48$, $\mu_z = 1.97$, $\epsilon_x = \epsilon_y = 2.34$, $\epsilon_z = 0.74$, $d = 3.1$ mm. Isotropic: $\epsilon_r = 2$ and $d = 2$ mm

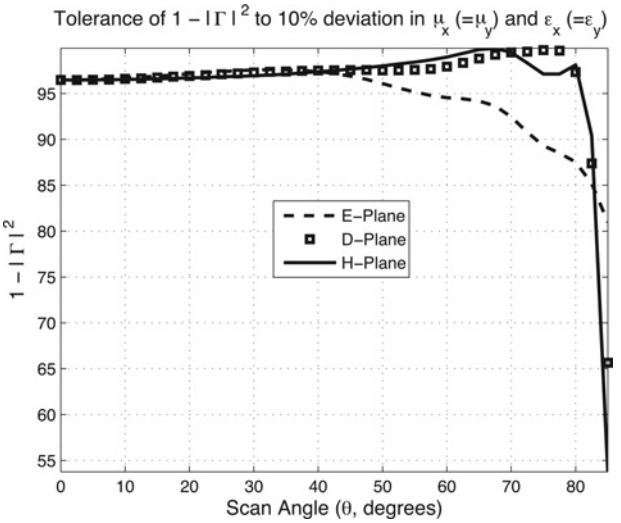

Figure 7 *Performance of the anisotropic WAIM of Figs. 4–6 when $\mu_x (= \mu_y)$ and $\epsilon_x (= \epsilon_y)$ deviate both by 10% from 1.48 and 2.34 to 1.63 and 2.1*

doi: 10.1049/iet-map.2009.0543

5 Simulation of electric L-C (ELC) metamaterial layer over phased-array antenna

In this section, we aim to demonstrate that a metamaterial layer can be used as a bonafide anisotropic WAIM layer. The examples presented in this section aim to verify the possibility of using metamaterials as anisotropic layers over the aperture plane of a phased-array antenna system.

5.1 Example 1

To verify the practicality of using an effective medium description to describe the behaviour of resonant structure-based metamaterials over a phased-array aperture junction, we simulate an ELC resonator metamaterial layer designed (a detailed description of ELC resonators can be found in [24]) to have effective medium parameters of $\mu_r = 1$, $\epsilon_x = \epsilon_y = 2.58$, $\epsilon_z = 1$ and $d = 2.1$ mm at the array operating frequency of 15.25 GHz. (Superficially ELC structures may bear resemblance to the four-legged FSS element [25], but conceptually they work in a different regime: the four-legged FSS element is used in a manner that puts it more in the bandgap of the dispersion diagram as opposed to the ELC, which is used at much longer wavelengths relative to the unit cell size, such that homogenisation applies.)

We thereafter compare these results with those from a simulation of an equivalently defined (in HFSS) homogeneous anisotropic material whose permeability and permittivity parameters are the same as that of the ELC metamaterial layer at 15.25 GHz.

Fig. 8 shows the topology of the metamaterial WAIM setup simulated in HFSS (a phased-array with a square lattice was used here (and in Example 2) to computationally accommodate the square-shaped ELCs; the lattice parameter of the phased-array square lattice is 10.5 mm), and also shows the constitutive parameter retrieval results for the ϵ_x and ϵ_y direction of the metamaterial. The retrieved results were derived from the scattering parameter matrix values using the method outlined in [26]. Although shaded differently in Fig. 8, the ELC layer is immersed in air (no other substrate) and was placed at a distance $d/2$ above the aperture; the shaded region in which the metamaterial layer is immersed has a total thickness, d, and is used in the parameter retrieval shown in Fig. 8. The metal trace on the ELC unit cell of Fig. 8 is of PEC material.

A comparison of the full-wave simulation of the array topology in Fig. 8 and that of an equivalently assigned homogeneous anisotropic material is shown in Fig. 9.

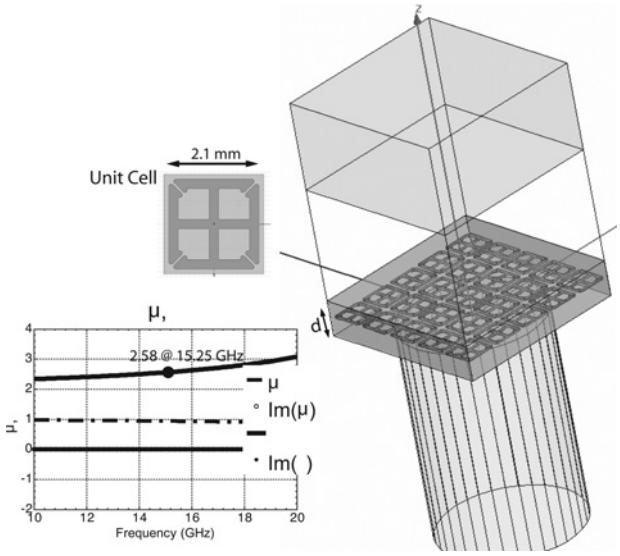

Figure 8 *Topology of phased-array unit lattice with ELC-based metamaterial layer*

5.2 Example 2

In this second example, an ELC-based metamaterial layer with parameters $\mu_r = 1$, $\epsilon_x = \epsilon_y = 1.9$, $\epsilon_z = 1$ and $d = 2.1$ mm placed 2.1 mm above the array is simulated and its results are compared to that of an equivalently assigned homogeneous anisotropic material. Fig. 10 shows the setup and unit cell characteristics of the ELC layer used herein.

A comparison of the HFSS simulation results for the ELC metamaterial layer and the equivalently assigned bulk anisotropic material is shown in Fig. 11. Note that the ELC array in this example is also made out of PEC and immersed completely in vacuum.

Figs. 9 and 11 show exact agreements between results obtained from the ELC WAIM simulations and

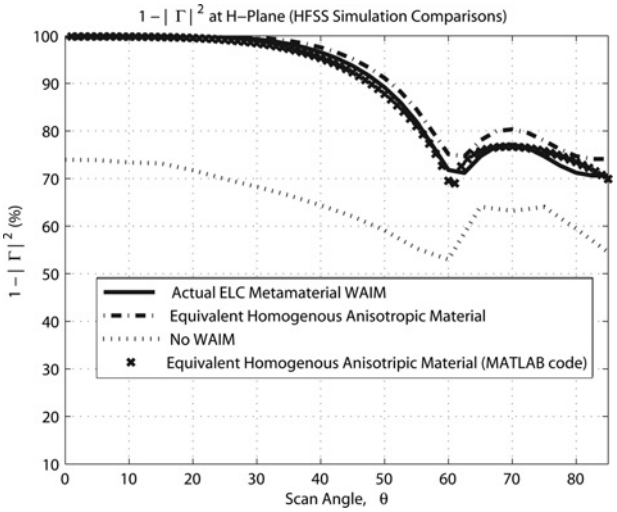

Figure 9 *Example 1: Comparisons of $1 - |\Gamma|^2$ for metamaterial layer against equivalent homogeneous anisotropic medium material ($\mu_r = 1$, $\epsilon_x = \epsilon_y = 2.58$, $\epsilon_z = 1$ and $d = 2.1$ mm) over array with square lattice*

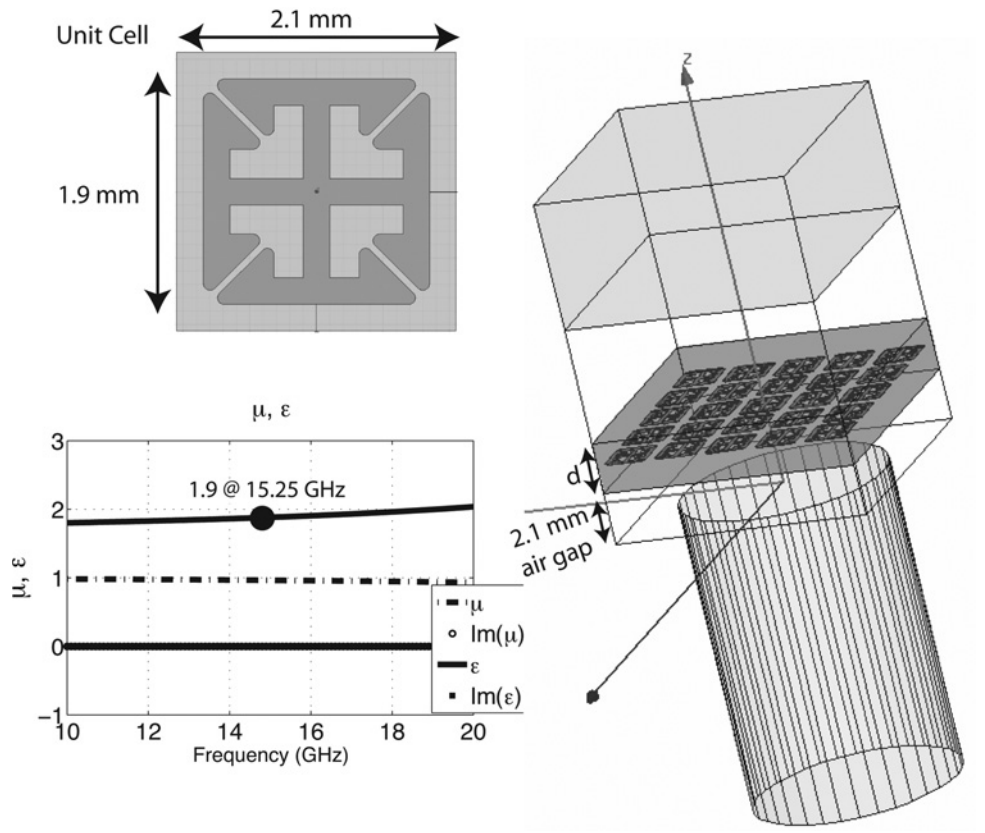

Figure 10 *Phased-array unit lattice with ELC-based metamaterial layer (with air gap over array)*

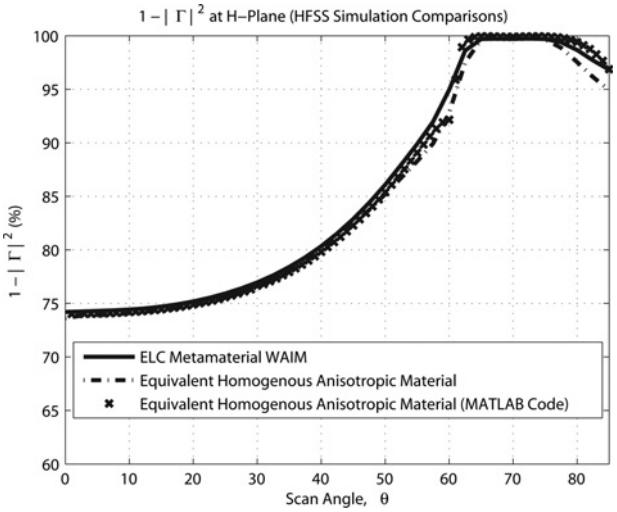

Figure 11 *Example 2: Comparisons of $1 - |\Gamma|^2$ for metamaterial layer against equivalent homogeneous anisotropic medium material ($\mu_r = 1$, $\epsilon_x = \epsilon_y = 1.9$, $\epsilon_z = 1$, and $d = 2.1$ mm) over array with square lattice*

that of the equivalent homogeneous anisotropic simulations. From the $(1 - |\Gamma|^2)$ agreements, it can be reasonably inferred that an effective medium model (homogenisation of the metamaterial array) sufficiently describes the behaviour of a metamaterial layer over the phased-array used here.

6 Bandwidth

Since bandwidth is a critical figure of merit in most microwave systems, it is important to consider the implications of metamaterial WAIMs on the bandwidth of phased-array antennas. Depending on the frequency regime within which a metamaterial is being used, its permittivity or permeabilty may change rapidly, especially at frequencies close to the metamaterial particle resonance. For the resonant ELC particles shown in Figs. 8 and 10, the resonance frequency is located at 34 and 36 GHz, respectively, and because of the large separation of the resonance frequency from the 15.25 GHz antenna operation frequency, we can operate in a less frequency dispersive and less lossy regime of the metamaterial. For instance, within the often used narrowband application explored herein (500 MHz surrounding the 15.25 GHz frequency), the permittivity $\epsilon_x = \epsilon_y$ varies only from 1.88 to 1.89 for the ELC in Example 1 and from 2.56 to 2.59 for the ELC in Example 2, thus exhibiting minimal dispersion within the bandwidth of the antenna.

When very large or very small constitutive parameter values are needed in a metamaterial however, it might be necessary to operate closer to the resonance frequency of the metamaterial, in which case high losses and strong frequency dispersion will be encountered. Based on these considerations, it would be important to optimise the WAIM parameters such that the anisotropic constitutive

doi: 10.1049/iet-map.2009.0543

parameters needed are neither very high nor near zero nor negative, as in these regimes strong frequency dispersion and large losses will be encountered.

7 Conclusion

We have suggested the use of anisotropic layers, implementable using metamaterials, to achieve wide angle impedance matching for phased-array antennas. In order to successfully achieve WAIM via this method, it would be essential to be able to reliably design metamaterial layers with at least four degrees of freedom (uniaxial μ, uniaxial ϵ, variable thickness). For a reliable and predictable design to be achieved, further work will need to be done so as to develop metamaterial structures with minimised loss, cross-coupling and bi-anisotropic effects [27]. Additionally, it would be important to utilise metamaterial structures that can be feasible and realisable from the fabrication standpoint. Although the aforementioned factors need to be taken into account during the metamaterial WAIM implementation process, this paper contributes to the foundational work needed to characterise arrays matched with anisotropic materials, and then presents numerical data that validates the prospects of using metamaterials to achieve anisotropic WAIMs.

8 Acknowledgment

This work was sponsored by DARPA contract # HR0011-05-C-0068.

9 References

[1] ZIOLKOWSKI R.W., ERENTOK A.: 'Metamaterial-based efficient electrically small antennas', *IEEE Trans. Antennas Propag.*, 2006, **54**, (7), pp. 2113–2130

[2] ALU A., ENGHETA N.: 'Pairing an epsilon-negative slab with a mu-negative slab: resonance, tunneling and transparency', *IEEE Trans. Antennas Propag.*, 2003, **51**, (10), pp. 2558–2571

[3] MASLOVSKI S., TRETYAKOV S.: 'Phase conjugation and perfect lensing', *J. Appl. Phys.*, 2003, **94**, (7), pp. 4241–4243

[4] LAI A., ITOH T., CALOZ C.: 'Composite right/left-handed transmission line metamaterials', *IEEE Microw. Mag.*, 2004, **5**, (3), pp. 34–50

[5] ELEFTHERIADES G.V., IYER A.K., KREMER P.C.: 'Planar negative refractive index media using periodically l-c loaded transmission lines', *IEEE Trans. Microw. Theory Tech.*, 2002, **50**, (12), pp. 2702–2712

[6] SMITH D.R., MOCK J.J., STARR A.F., SCHURIG D.: 'Gradient index metamaterials', *Phys. Rev. E*, 2005, **71**, (3), article id 036609

[7] SHELBY R.A., SMITH D.R., SCHULTZ S.: 'Experimental verification of a negative index of refraction', *Science*, 2001, **292**, (5514), pp. 77–79

[8] SMITH D.R., PADILLA W.J., VIER D.C., NEMAT-NASSER S.C., SCHULTZ S.: 'Composite medium with simultaneously negative permeability and permittivity', *Phys. Rev. Lett.*, 2000, **84**, (18), pp. 4184–4187

[9] SCHURIG D., MOCK J.J., JUSTICE B.J., *ET AL.*: 'Metamaterial electromagnetic cloak at microwave frequencies', *Science*, 2006, **314**, (5801), pp. 977–980

[10] MAGILL E., WHEELER H.: 'Wide-angle impedance matching of a planar array antenna by a dielectric sheet', *IEEE Trans. Antennas Propag. [legacy, pre – 1988]*, 1966, **14**, (1), pp. 49–53

[11] KISHK A.A., CHAIR R., LEE K.F.: 'Experimental investigation for wideband perforated dielectric resonator antenna', *IEEE Electron. Lett.*, 2006, **33**, (6), pp. 137–139

[12] WU C.P., AMITAY N., GALINDO V.: 'Theory and analysis of phased-array antennas' (Wiley Interscience, 1972)

[13] STARK L.: 'Microwave theory of phased-array antennas – a review', *Proc. IEEE*, 1974, **62**, (12), pp. 1661–1701

[14] MAILLOUX R.J.: 'Phased-array antenna handbook' (Artech House, 2005, 2nd edn.)

[15] STARK L.: 'Radiation impedance of a dipole in an infinite planar phased-array', *Radio Sci.*, 1966, **3**, pp. 361–375

[16] FARRELL G. JR, KUHN D.: 'Mutual coupling in infinite planar arrays of rectangular waveguide horns', *IEEE Trans. Antennas Propag. [legacy, pre – 1988]*, 1968, **16**, (4), pp. 405–414

[17] PARAD L.: 'The input admittance to a slotted array with or without a dielectric sheet', *IEEE Trans. Antennas Propag. [legacy, pre – 1988]*, 1967, **15**, (2), pp. 302–304

[18] WHEELER H.: 'The grating-lobe series for the impedance variation in a planar phased-array antenna', *IEEE Trans. Antennas Propagat. [legacy, pre – 1988]*, 1966, **14**, (6), pp. 707–714

[19] MUNK B.A.: 'Finite antenna arrays and FSS' (Wiley Interscience, 2003, 1st edn.)

[20] BORGIOTTI G.V.: 'Modal analysis of periodic planar phased arrays of apertures', *Proc. IEEE*, 1968, **56**, (11), pp. 1881–1892

[21] LANNE M.: 'An analysis of a finite array using infinite array data'. Technical report, Chalmers University of Technology, Ericsson Microwave Systems AB, 2004

[22] POZAR D.M.: 'Microwave engineering' (Wiley Publishers, 2005, 3rd edn.)

[23] BORGIOTTI G.: 'Radiation and reactive energy of aperture antennas', *IEEE Trans. Antennas Propag. [legacy, pre – 1988]*, 1963, **11**, (1), pp. 94–95

[24] SCHURIG D., MOCK J.J., SMITH D.R.: 'Electric-field-coupled resonators for negative permittivity metamaterials', *Appl. Phys. Lett.*, 2006, **88**, (4), article id 041109

[25] MUNK B.A.: 'Frequency selective surfaces' (Wiley Interscience, 2000, 1st edn.)

[26] SMITH D.R., SCHULTZ S., MARKOŠ P., SOUKOULIS C.M.: 'Determination of effective permittivity and permeability of metamaterials from reflection and transmission coefficients', *Phys. Rev. B*, 2002, **65**, (19), article id 195104

[27] MARQUÉS R., MEDINA F., RAFII-EL-IDRISSI R.: 'Role of bianisotropy in negative permeability and left-handed metamaterials', *Phys. Rev. B*, 2002, **65**, (14), article id 144440

10 Appendix

We can express the tangential fields at the array surface in two ways: (i) as consisting of a summation of the field distribution of an infinitum of waveguide modes, and (ii) as consisting of a summation of the field distribution of free space modes excited at the aperture interface. We will express these summation symbolically and equate them in order to enforce the tangential electric and magnetic field boundary conditions at the array surface (i.e. the $z = 0$ plane).

Using a bidimensional Floquet expansion (2D counterpart of Bloch's theorem), the tangential waveguide electric fields at $z = 0^+$ (i.e. just above the the $z = 0$ plane) can be represented as an excited spectrum of spatial harmonics weighted by vector coefficients $\boldsymbol{A}(\boldsymbol{u}_{opq})$

$$\boldsymbol{E}_t(\boldsymbol{x}) = \sum_{p=-\infty}^{+\infty} \sum_{q=-\infty}^{+\infty} \boldsymbol{A}(\boldsymbol{u}_{opq}) \mathrm{e}^{-\mathrm{j}\boldsymbol{u}_{opq}\cdot\boldsymbol{x}} \tag{19}$$

Representing the field distribution of waveguide mode i as $\boldsymbol{e}_i$, the tangential electric fields excited at $z = 0^-$ can be written as a sum of an infinitum of waveguide field distributions weighted by mode amplitudes V_i

$$\boldsymbol{E}_t(\boldsymbol{x}) = \sum_{i=0}^{\infty} V_i \boldsymbol{e}_i(\boldsymbol{x}) \tag{20}$$

The indices of waveguide modes start from $i = 0$ (the fundamental lone propagating waveguide mode), through $i = 1$ (the first higher order mode), to $i = \infty$ (the higher order mode at infinity). To enforce the boundary condition on the tangential electric fields at the array surface, expression (19) for $z = 0^+$ must equal (20) for $z = 0^-$. For a unit waveguide element, this takes the form

$$\boldsymbol{E}_t(\boldsymbol{x}) = \sum_{i=0}^{\infty} V_i \boldsymbol{e}_i(\boldsymbol{x}) = \sum_{p=-\infty}^{+\infty} \sum_{q=-\infty}^{+\infty} \boldsymbol{A}(\boldsymbol{u}_{opq}) \mathrm{e}^{-\mathrm{j}\boldsymbol{u}_{opq}\cdot\boldsymbol{x}} \tag{21}$$

As shown in (22), the same can be done for the tangential magnetic fields. For the sake of notational brevity, we refer to the active element admittance as Y_{in} instead of $Y_{\mathrm{in}}(\theta, \phi)$.

$$\hat{z} \times \left[Y_{\mathrm{in}} V_0 \boldsymbol{e}_{\mathrm{o}}(\boldsymbol{x}) - \sum_{i=1}^{\infty} Y_i V_i \boldsymbol{e}_i \right] = \sum_{p=-\infty}^{+\infty} \sum_{q=-\infty}^{+\infty} \boldsymbol{B}(\boldsymbol{u}_{opq}) \mathrm{e}^{-\mathrm{j}\boldsymbol{u}_{opq}\cdot\boldsymbol{x}} \tag{22}$$

The active element admittance Y_{in} is derived after expressing $\boldsymbol{A}(\boldsymbol{u}_{opq})$ and $\boldsymbol{B}(\boldsymbol{u}_{opq})$ in terms of the combination of plane wave admittances and a summation of the Fourier transforms of several waveguide modes. Reference [20] provides further detail.

doi: 10.1049/iet-map.2009.0543